Falling liquid films: wave patterns and thermocapillary effects

Benoit Scheid

Chimie-Physique E.P., Université Libre de Bruxelles C.P. 165/62
Avenue F.D. Roosevelt, 50 - 1050 Bruxelles - BELGIUM
E-mail: bscheid@ulb.ac.be

Abstract

Three-dimensional waves in film flows down a uniformly heated plane are investigated by simulation. For small Reynolds number, regularly spaced rivulets are observed, aligned with the flow and sustaining two-dimensional waves of larger amplitude and phase speed than in isothermal conditions. For larger Reynolds number, the picture is similar to the isothermal case and no rivulets appear. The transition between these two regimes shows complex cooperative behavior between both hydrodynamic and thermocapillary modes.

Key words: Falling film, Hydrodynamic instability, Thermocapillary effect

1 Introduction

Three-dimensional (3D) hydrodynamic waves in falling films have been investigated experimentally by various authors (see for instance [1]). Experiments by Liu & Gollub [4] and more recently by Park & Nosoko [5] give the clearest picture of the wide phenomenology of the interacting 3D waves on isothermal film flows such as synchronously deformed fronts, subharmonic patterns and horseshoe-like waves. Theoretically, we have applied a regularization procedure to the weighted integral boundary layer method providing a two-dimensional modeling that describe the complex wave patterns observed in experiments up to moderate Reynolds numbers [8]. For heated walls, Joo *et al.* [3] have modeled rivulet patterns induced by thermocapillary effects for small Reynolds number, i.e. using a single evolution equation for the film thickness. However their simulations experienced finite-time blow-up that was shown to be intrinsic to the Benney-type equation. Indeed, Ramaswamy *et al.* [6] have simulated the full three-dimensional boundary layer equations and could resolve the whole dynamics of a rivulet formation, from onset to rupture. Nevertheless, they were restricted to a domain size of about one wavelength in both streamwise and spanwise directions. We aim in this paper to propose a two-dimensional model describing the three-dimensional dynamics of a heated falling film in large-scale domains and to investigate the influence of the Marangoni effect on wave patterns observed in isothermal conditions up to moderate Reynolds number. We will in fact extend to 3D case the model developed by Ruyer-Quil *et al.* [7] for two-dimensional waves.

2 Mathematical formulation of the problem

The flow of a Newtonian liquid down a heated vertical plane is considered. We look for 2D equations in the streamwise (x) and spanwise (z) coordinates that mimic the full 3D motion of the fluid. Including the heating of the plane into the regularized three-field model –as detailed in [8]– leads to a four-field model independent on the cross-stream coordinate (y), for the film thickness h, the streamwise and spanwise flow rates q and p and the temperature field at the interface θ:

$$\partial_t h = -\partial_x q - \partial_z p\,, \tag{1a}$$

$$\begin{aligned}\delta\,\partial_t q = {} & \delta\left[\frac{9}{7}\frac{q^2}{h^2}\partial_x h - \frac{17}{7}\frac{q}{h}\partial_x q\right] + \left\{\delta\left[-\frac{8}{7}\frac{q\partial_z p}{h} - \frac{9}{7}\frac{p\partial_z q}{h} + \frac{9}{7}\frac{qp\partial_z h}{h^2}\right] + \frac{5}{6}h - \frac{5}{2}\frac{q}{h^2}\right. \\ & +\eta\left[4\frac{q\left(\partial_x h\right)^2}{h^2} - \frac{9}{2}\frac{\partial_x q\partial_x h}{h} - \frac{13}{16}\frac{\partial_z p\partial_x h}{h} - \frac{43}{16}\frac{\partial_x p\partial_z h}{h} - \frac{73}{16}\frac{p\partial_{xz} h}{h} - 6\frac{q\partial_{xx} h}{h}\right. \\ & \left.-\frac{\partial_z q\partial_z h}{h} + \frac{3}{4}\frac{q\left(\partial_z h\right)^2}{h^2} + \frac{13}{4}\frac{p\partial_x h\partial_z h}{h^2} - \frac{23}{16}\frac{q\partial_{zz} h}{h} + \frac{9}{2}\partial_{xx} q + \partial_{zz} q + \frac{7}{2}\partial_{xz} p\right] \\ & \left.-\mathcal{M}\left(\frac{5}{4}\partial_x\theta - \frac{\delta}{224}hq\partial_{xx}\theta\right) + \frac{5}{6}h\left(\partial_{xxx} h + \partial_{xzz} h\right)\right\} \\ & \times\left(1 - \frac{\delta}{70}q\partial_x h + \mathcal{M}\frac{5}{56}\frac{\partial_x\theta}{h}\right)^{-1},\end{aligned} \tag{1b}$$

$$\begin{aligned}\delta\,\partial_t p = {} & \delta\left[\frac{9}{7}\frac{p^2}{h^2}\partial_z h - \frac{17}{7}\frac{p}{h}\partial_z p - \frac{8}{7}\frac{p\partial_x q}{h} - \frac{9}{7}\frac{q\partial_x p}{h} + \frac{9}{7}\frac{qp\partial_x h}{h^2}\right] - \frac{5}{2}\frac{p}{h^2} \\ & +\eta\left[4\frac{p\left(\partial_z h\right)^2}{h^2} - \frac{9}{2}\frac{\partial_z p\partial_z h}{h} - \frac{13}{16}\frac{\partial_x q\partial_z h}{h} - \frac{43}{16}\frac{\partial_z q\partial_x h}{h} - \frac{73}{16}\frac{q\partial_{xz} h}{h} - 6\frac{p\partial_{zz} h}{h}\right. \\ & \left.-\frac{\partial_x p\partial_x h}{h} + \frac{3}{4}\frac{p\left(\partial_x h\right)^2}{h^2} + \frac{13}{4}\frac{q\partial_x h\partial_z h}{h^2} - \frac{23}{16}\frac{p\partial_{xx} h}{h} + \frac{9}{2}\partial_{zz} p + \partial_{xx} p + \frac{7}{2}\partial_{xz} q\right] \\ & -\frac{5}{4}\mathcal{M}\partial_z\theta + \frac{5}{6}h\left(\partial_{xxz} h + \partial_{zzz} h\right)\,,\end{aligned} \tag{1c}$$

$$\begin{aligned}\delta\,\partial_t\theta = {} & 3\frac{(1-\theta-Bh\theta)}{Prh^2} + \delta\left[\frac{7}{40}(1-\theta)\frac{(\partial_x q + \partial_z p)}{h} - \frac{27}{20}\frac{(q\partial_x\theta + p\partial_z\theta)}{h}\right] \\ & +\frac{\eta}{Pr}\left[\left(1-\theta-\frac{3}{2}Bh\theta\right)\left(\frac{(\partial_x h)^2}{h^2} + \frac{(\partial_z h)^2}{h^2}\right) + \frac{\partial_x h\partial_x\theta}{h} + \frac{\partial_z h\partial_z\theta}{h}\right. \\ & \left.+(1-\theta)\frac{(\partial_{xx} h + \partial_{zz} h)}{h} + \partial_{xx}\theta + \partial_{zz}\theta\right]\,,\end{aligned} \tag{1d}$$

where the reduced dimensionless numbers are

$$\delta = \frac{(3Re)^{11/9}}{\Gamma^{1/3}}\,,\quad B = Bi\,(3Re)^{1/3}\,,\quad \mathcal{M} = \frac{Ma}{\Gamma^{1/3}(3Re)^{4/9}}\quad\text{and}\quad \eta = \frac{(3Re)^{4/9}}{\Gamma^{2/3}}\,,$$

based in turn on the usual Reynolds, Biot, Marangoni and Kapitza numbers:

$$Re = \frac{g h_{\mathrm{N}}^3}{3\nu^2}\,, \quad Bi = \frac{\alpha \nu^{2/3}}{\lambda g^{1/3}}\,, \quad Ma = \frac{\gamma \Delta T}{\rho \nu^{4/3} g^{1/3}} \quad \text{and} \quad \Gamma = \frac{\sigma}{\rho \nu^{4/3} g^{1/3}}\,,$$

with g the gravity acceleration, h_{N} the thickness of the uniform film, ν the kinematic viscosity, ρ the density, σ the surface tension, $\gamma = -\mathrm{d}\sigma/\mathrm{d}T$, α the heat transfer coefficient and λ the thermal conductivity; $Pr = \nu/\chi$ is the Prandtl number where χ is the thermal diffusivity. The lengthscales are h_{N} and $h_{\mathrm{N}}/\sqrt{\eta}$ in the wall-normal y and in the in-plane x and z directions, respectively, while the timescale is $\nu/g h_{\mathrm{N}}\sqrt{\eta}$. Equation (1a) is the mass conservation equation, equations (1b,1c) express the averaged momentum balances in both directions x and z, and equation (1d) is the energy balance.

3 Computations

3.1 Small-size domain

We first validate our model with a small-scale simulation investigated by Ramaswamy *et al.* [6] for small Reynolds numbers, i.e. when a one-field model can still be valid. They demonstrated a mechanism of rivulet formation based solely on instability phenomena. Figure 1 shows simulation results, done with periodic boundary conditions and a simple harmonic disturbance of the form $h(x, z, 0) = 1 + 0.1\cos(k_x\, x) + 0.1\cos(k_z\, z)$, as initial condition. The wavenumbers k_x and k_z have been chosen to be below those for the maximal linear growth rate in each direction, which are $k_{x\max} = 0.56$ and $k_{z\max} = 0.53$. Actually, these appropriate values allow for interesting secondary flow development. The initial perturbation creates a trough in the center of the domain (a). Then, thermocapillarity sets in, displacing the fluid from the hotter troughs towards the surrounding colder crests. However, the growth rate of the hydrodynamic mode is dominant at initial stage and surface waves develop (b). The local phase speed being proportional to the square of the local film thickness, the crest travel faster than the trough (c). In the absence of the mean flow in the spanwise direction, the liquid is displaced laterally due to thermocapillarity. Therefore, as time progresses, the thinning of the liquid layer persists and forms a valley surrounded by rivulets aligned with the flow (d). This process is similar to the evolution of a heated thin film on a horizontal substrate. Likewise, it exhibits the formation of a secondary rivulet between the main one (e). As found by Boos & Thess [2] for horizontal layers, a true 'cascade of structures' takes place in thinner zones (f), precursor to the film rupture. The last stage before rupture obtained by Ramaswamy *et al.* with DNS is at $t = 153$, which is in excellent agreement with Fig.1*e*. However, our simulation runs beyond this time and exhibits finer structures in the film before its rupture (see Fig.1*g*). The reason why the full-scale computations with Navier-Stokes/Fourier equations did not provide such further evolution

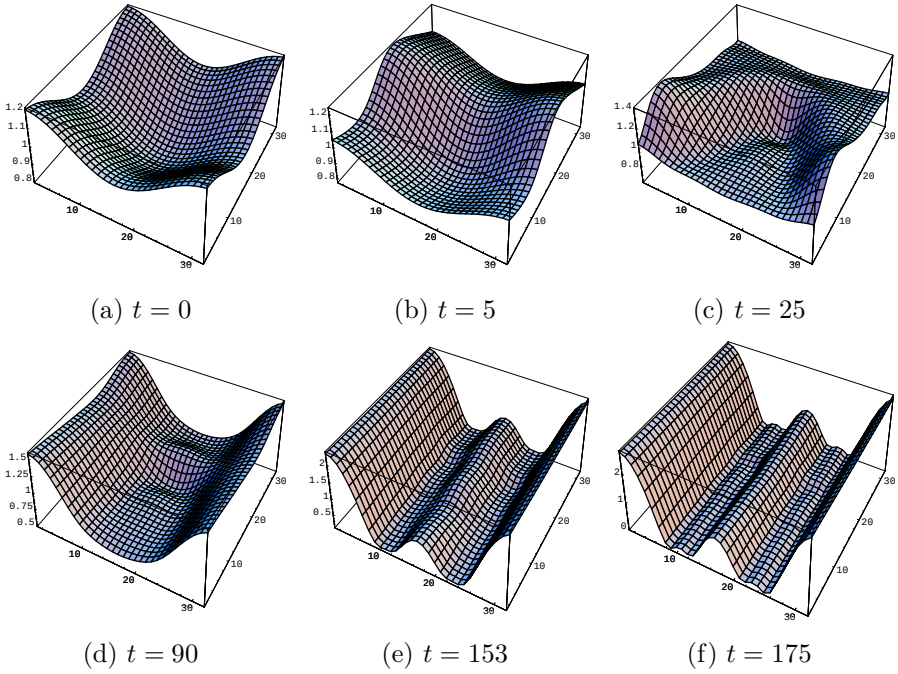

(a) $t = 0$ (b) $t = 5$ (c) $t = 25$

(d) $t = 90$ (e) $t = 153$ (f) $t = 175$

Figure 1: Inception and development of rivulet aligned with the flow computed with (1) arising for $Re = 1/3$, $\Gamma = 300$, $Ma = 10$, $Bi = 1$ and $Pr = 7$. The domain is square of side $2\pi/k_x$ with $k_x = k_z = 0.335$. The flow direction is from the right top towards the left bottom.

of the film is likely related to the choice of the number of mesh points used in [6]. The authors would have most probably been able to compute larger time with refined grid resolution. However, this would have been at the expense of computing time, which demonstrate the great advantage of working with a model of reduced dimensionality. Indeed, our reduced model involves variables that are defined only at the film surface and not in the bulk. Actually, the mesh points are 32×32 and the time necessary for computing the case of Fig.1, with an accuracy of 10^{-4}, is about one hour on a standard desktop computer.

Now, let increase the Reynolds number up to $Re = 2$, i.e. out of the range of validity of a single evolution equation for the film thickness. The wavenumbers for the maximal linear growth rate are $k_{x\max} \approx 0.62$ and $k_{z\max} \approx 0.34$ (approximated values calculated in the long-wave limit), which yields $k_x \sim k_{x\max}/2$ while $k_z \sim k_{z\max}$. Figure 2 shows that the hydrodynamic mode quickly generates high amplitude waves (a,b) that evolves to a solitary-like wave with preceding capillary ripples (c). However, the thermocapillary mode leads the film to rupture before the surface wave saturates. An interesting interaction between the two modes can be pointed out here: as the thermocapillary flow feeds the core of the rivulet, the mean film thickness at the crest increases, and so the local flow rate. Hence, the wave solution

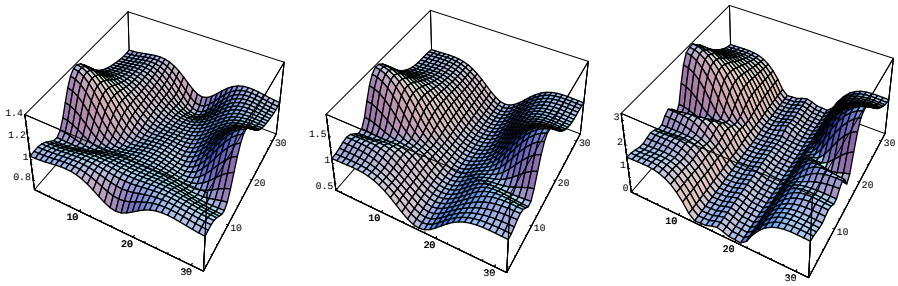

(a) $t = 40$ (b) $t = 400$ (c) $t = 690$

Figure 2: Same as for Fig.1 with $Re = 2$.

does not saturate and rather follows the change of the 'local Reynolds number', by increasing its amplitude and its phase speed. This process vanishes at $t > 620$ when the film approaches the wall enough for the viscous stress to slow down the lateral thermocapillary flow. The hydrodynamic wave and the longitudinal rivulet were found to coexist along a distance that is about 50 wavelengths here and that increases with Re.

3.2 Large-size domain

Let us turn now to large-scale simulations of a water film at 20°C ($\Gamma = 3375$, $Pr = 7$) with a temperature difference between the vertical wall and the ambient air of 5°C ($Ma = 50$) and a high heat transfer coefficient of 1000W/cm^{2}K ($Bi = 0.1$). The simulations that follow were started with a white noise of amplitude 1/1000 of the flat film thickness. Figure 3 shows again the formation of rivulets due to Marangoni effect: after the development of a parallel wave train (a), drop-like accumulation breaks the 2D waves into 3D patterns (b,c), precursor of rivulet patterns aligned with the flow (d,e). As depicted previously for Fig.2, the liquid then accumulates into rivulets, which increases the 'local Reynolds number' and fosters 2D solitary-like waves of larger amplitude and phase speed than in isothermal conditions (f). This process continues until the rupture of the film, the snapshot of which is shown in Fig.4*a*. Similar rivulet pattern, but with larger wavelength, is also shown for $Re = 5$ (b) while no rivulet develops for still larger $Re = 10$ (c) where the wave pattern behaves like in isothermal conditions [5].
Figure 5 shows finally the phase speed of solitary waves versus Re. For small Reynolds number and small phase speed, i.e. in the *drag-gravity regime*, inertia effects are small as compared to thermocapillary effects while it is the contrary for large Reynolds number and large phase speed, i.e. in the *drag-inertia regime*, where inertia is dominant. The resulting patterns are drastically different (a,c). The transition between these two regimes for $4 < Re < 6$ shows complex cooperative behavior between both hydrodynamic and thermocapillary modes, mostly when their

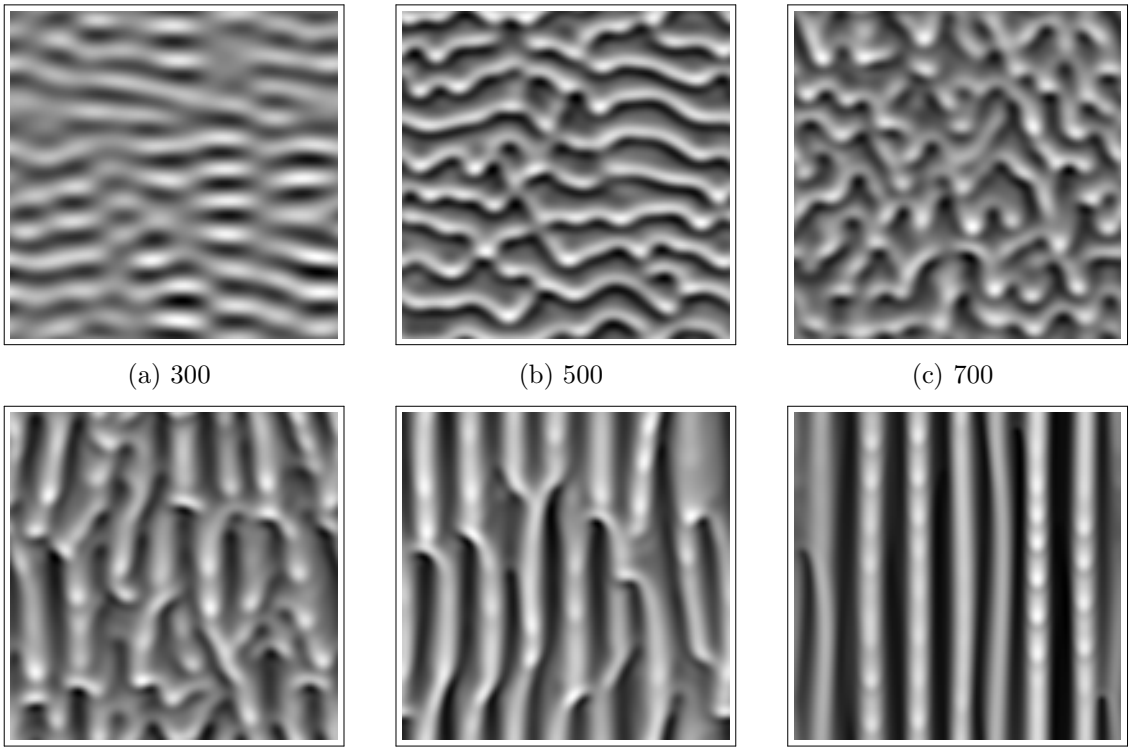

(a) 300 (b) 500 (c) 700

(d) 900 (e) 1100 (f) 1500

Figure 3: Water film free surface at different time for $Re = 2$ for $Ma = 50$, $Bi = 0.1$, $Pr = 7$ and $\Gamma = 3375$. The domain is a square of side $2\pi/k_x$ where $k_x = k_z = 0.05$. Bright (resp. dark) zones correspond to elevations (resp. depressions).

amplitudes are comparable, as illustrated for $Re = 5$ in Fig.4*b*.

4 Discussion

The dynamical coupled equations for the film thickness h, the surface temperature θ and the streamwise and spanwise flow rates q and p given in (1) has been shown to be robust and accurate in describing the competition between hydrodynamic waves and thermocapillary effect responsible for the rivulet formation in heated falling liquid films.

For constant temperature difference across the film, it has been found that in the drag-gravity regime, quasi-regularly spaced rivulets arise and grow up until rupture (a). Meanwhile, the rivulet confines the flow in such a way that waves behaves like two-dimensional solitary waves, but of higher flow rate because of the local increase of the Reynolds number. On the contrary, no qualitative influence of the Marangoni effect has been observed in the drag-inertia regime, at least during the

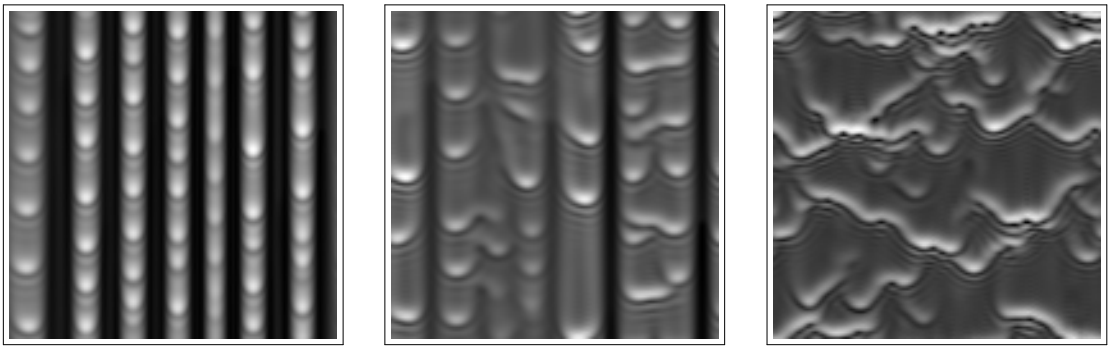

(a) $Re = 2$ (b) $Re = 5$ (c) $Re = 10$

Figure 4: Wave patterns for $Ma = 50$, $Bi = 0.1$, $Pr = 7$ and $\Gamma = 3375$.

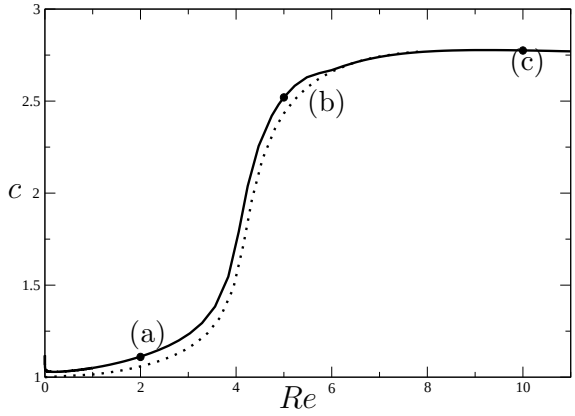

Figure 5: Phase speed c of solitary waves versus Re for $Ma = 50$ (solid line) and $Ma = 0$ (dashed line). The letters refer to Fig.4.

time of the simulations, showing that inertia fully dominates the dynamics of the film (c). Finally the transition between these two regimes is also instructive in terms of rupture which occurs at only one place and not between all rivulets at the same time. This is due to the dispersion of the rivulet size and amplitude, allowing also to observe different kind of waves: 2D wave trains, 2D solitary waves and 3D wave structure (b).

Having at one's disposal reliable low-dimension model, one is now able to undergo systematic numerical analyzes at low cost (in terms of CPU time) and for large domains. This will allow to explore in the whole parameter space the complex 3D interactions between hydrodynamic and thermocapillary effects. Notice however that, to our knowledge, no experimental data of film flowing down uniformly heated substrates are yet available for comparison purpose.

Acknowledgment

The author would like to thank Serafim Kalliadasis and Christian Ruyer-Quil for fruitful discussions.

References

[1] S.V. Alekseenko, V.E. Nakoryakov, and B.G. Pokusaev. *Wave flow in liquid films*. Begell House (New York), third edition, 1994.

[2] W. Boos and A. Thess. Cascade of structures in long-wavelength marangoni instability. *Phys. Fluids*, 11:1633, 1999.

[3] S.W. Joo and S.H. Davis. Instabilities of three-dimensional theory viscous falling films. *J. Fluid Mech.*, 242:529, 1992.

[4] J. Liu, J.B. Schneider, and J.P. Gollub. Three-dimensional instabilities of film flows. *Phys. Fluids*, 7:55–67, 1995.

[5] C. D. Park and T. Nosoko. Three-dimensional wave dynamics on a falling film and associated mass transfer. *AIChE J.*, 49(11):2715–2727, 2003.

[6] B. Ramaswamy, S. Krishnamoorthy, and S.W. Joo. Three-dimensional simulation of instabilities and rivulet formation in heated falling films. *J. Comp. Phys.*, 131:70–88, 1997.

[7] C. Ruyer-Quil, B. Scheid, S. Kalliadasis, M.G. Velarde, and R.Kh. Zeytounian. Thermocapillary long waves in a liquid film flow. part 1. low dimensional formulation. *J. Fluid Mech.*, 538:199–222, 2005.

[8] B. Scheid, C. Ruyer-Quil, and P. Manneville. Wave patterns in film flows: Modelling and three-dimensional waves. *J. Fluid Mech., to appear*, 2006.